# Time-domain measurements reveal spatial aberrations in a sub-surface two-photon microscope

**M. RUTKAUSKAS,[1,*] D. T. REID,[1] J. GARDUÑO-MEJÍA[2], M. ROSETE-AGUILAR[2]**

[1]*Scottish Universities Physics Alliance (SUPA), Institute of Photonics and Quantum Sciences, School of Engineering and Physical Sciences, Heriot-Watt University, Riccarton, Edinburgh EH14 4AS, UK*
[2]*Centro de Ciencias Aplicadas y Desarrollo Tecnológico, Universidad Nacional Autónoma de México, Av. Universidad 3000, Coyoacán, Distrito Federal 04510, México.*
**Corresponding author: M.Rutkauskas@hw.ac.uk*

Received XX Month XXXX; revised XX Month, XXXX; accepted XX Month XXXX; posted XX Month XXXX (Doc. ID XXXXX); published XX Month XXXX

**We show that in a nonlinear microscopy system the effects of chromatic and spherical aberrations are revealed by a difference in the focal positions corresponding to the shortest pulse duration and the minimum lateral resolution. By interpreting experimental results from a high-numerical-aperture two-photon microscope using a previously reported spatio-temporal model, we conclude that the two-photon autocorrelation of the pulses at the focal plane can be used to minimize both the chromatic and spherical aberrations of the system. Based on these results, a possible optimization strategy is proposed whereby the objective lens is first adjusted for minimum autocorrelation duration, then the wavefront before the objective is modified to maximize the autocorrelation intensity.** 

***OCIS codes: (110.0110) Imaging systems; (180.4315) Nonlinear microscopy; (320.0320) Ultrafast optics; (320.5540) Pulse shaping; (320.5550) Pulses.***

http://dx.doi.org/10.1364/AO.99.099999

## 1. INTRODUCTION

Modern microscope objective lenses are normally well corrected for all spatial aberrations, however in certain implementations, such as deep sub-surface microscopy, aberrations arise elsewhere in the imaging system which were not anticipated in the original lens design. Existing aberration estimation and compensation techniques take many forms, but can be characterized as sensor-based and sensor-free. Guide-star methods have been used successfully in two-photon fluorescence microscopy, and proceed by generating a point source of fluorescence whose wavefront aberrations can be detected by a Shack-Hartmann sensor [1]. While very effective for fluorescence microscopy, this approach cannot be extended to two-photon optical beam induced current microscopy because no fluorescence signal is generated in this microscopy modality. In the absence of a fluorescence signal, sensor-free approaches are needed. Previous examples include optimizing the image quality metric based upon the low spatial frequency content of the image [2] or by making intensity measurements under different compensation conditions [3]. In this paper we show how time-domain measurements made using the nonlinear response of the sample itself can be used to reveal the presence of aberrations, and potentially inform a new aberration compensation strategy.

In a nonlinear microscope using femtosecond pulses to illuminate the sample, uncorrected spatial aberrations not only degrade the lateral and axial resolution of the system, but also couple into the time domain to stretch the pulses beyond their minimum transform-limited durations [4]. In particular, two common spatial aberrations significantly affect the pulse durations: chromatic aberration remaps the arrival times at the focal plane of the different colors in the pulse, while spherical aberration leads to another remapping based on the radial position of components of the pulse [5]. This insight led us to examine the question of whether time-domain measurements could be applied to diagnose the presence of spatial aberrations, and even to inform an experimental strategy for minimizing their impact.

The context of this work is the sub-surface microscopy of complementary metal-oxide semiconductor (CMOS) integrated circuits (ICs), whose progressively decreasing feature sizes mean that optical solutions for spatial fault localization in these devices are continually challenged to maintain sufficient resolving power. Nonlinear microscopy has been applied to sub-surface imaging of CMOS ICs using the two-photon optical beam induced current (TOBIC) technique [6-8], and also for fault localization using the two-photon laser-assisted device alteration (2pLADA) method [9-11]. In both scenarios, optical resolutions of around 100 nm have been achieved by combining solid-immersion lens (SIL) imaging [12]—which provides an exceptionally high numerical aperture (NA)—with the $\sqrt{2}$ reduction in the lateral point-spread function achieved by two-photon excitation [13].

Optically-based fault localization normally proceeds by imaging through the silicon substrate of the IC and into the device layer of the chip, because frontside imaging is no longer practical due to the multitude of metallization layers which obscure access from this direction in modern devices. SIL microscopy in a high refractive index

medium like silicon ($n$ = 3.48) requires the dimensions of the SIL to be precisely fabricated for a given substrate thickness (typically around 100 µm), otherwise spherical aberrations will be encountered [14]. The type of SIL used (i.e. central or aplanatic) determines the severity of tolerancing errors in the SIL design or non-uniformity in the substrate thickness [15]. It is commonly observed that the aplanatic design, while generally providing superior resolving power to the central SIL, is substantially (around 10×) more sensitive to fabrication errors than the central SIL [15], meaning that uncorrected aberrations may remain in a system which was otherwise correctly designed. It is in this context that techniques to identify and even mitigate aberrations in the system are important.

## 2. MICROSCOPE SYSTEM

### A. Solid Immersion Lens Microscope

Illuminated with near-infrared femtosecond pulses, the microscope used the TOBIC effect to produce images, which are maps of the photocurrent generated by the device as the location of the focal spot is raster-scanned across the chip. The TOBIC signal depends quadratically on incident peak intensity [6], so the CMOS device itself provides a nonlinear response which is suitable for pulse-duration estimation by recording $g_2(\tau)$, the interferometric second-order autocorrelation profile [16]. By inferring the autocorrelation width at the focal plane it is possible to compensate and manipulate the pulse chirp before entering the pupil of the focusing optics. This offers a way of reducing the durations of the laser pulses while providing aberration free imaging at the focal plane and maximizing the two-photon signal. As we show later with measurements of the lateral imaging resolution, the autocorrelation durations recorded at out-of-focus planes provide a metric which could be used to find optimal focusing by conducting a sequence of rapid autocorrelation measurements.

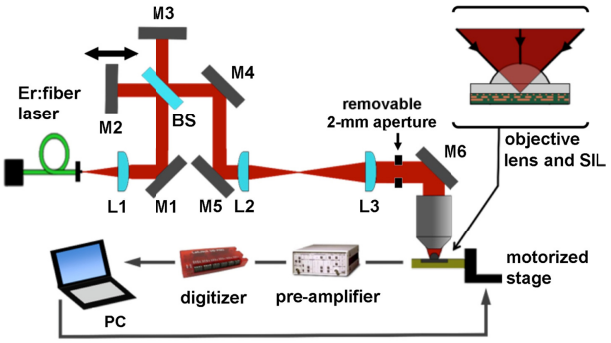


Fig. 1. TOBIC microscope. See text for details.

The experimental set-up is illustrated in Fig. 1. A femtosecond Er:fiber laser operating at 1550 nm wavelength was employed to perform the TOBIC microscopy. Immediately before the microscope the pulses had durations of 144 fs (with a moderate chirp to pre-compensate dispersion in the microscope optics), a repetition rate of 68 MHz and an average power of 200 mW. The beam from the Er:fiber laser was collimated by lens L1 before entering a Michelson interferometer in which the pulses were split into two time-delayed replicas which could later be recombined in the device to yield the interferometric autocorrelation function. At the output of the interferometer the beam was expanded to a diameter of 9.8 mm using a telescope (lenses L2 and L3) to overfill the 8.4-mm-diameter pupil of the microscope objective (NA 0.42, 20×). An adjustable aperture was inserted immediately before the objective lens to allow spherical aberration to be diagnosed by performing finite-aperture experiments in which the NA of the imaging system was moderately reduced. To conduct the resolution measurements without interference effects we blocked the moving mirror M2 in the Michelson interferometer.

The nonlinear TOBIC microscope incorporated a silicon central SIL, which takes advantage of the first aplanatic point of the sphere [12]. The diameter of the SIL was chosen to be 4 mm and it was cut to a height of 1.73 mm. This SIL design allowed us to image deep inside the silicon substrate. The design and the basic working principle of the SIL are shown in Fig. 2a. The inclusion of the silicon SIL in the imaging system enhanced the NA of the microscope by a multiple of the refractive index of silicon (3.48) to NA 1.46.

The device used for the experiments was a 350-nm-feature-size CMOS IC. Imaging was performed through the backside of the device, which covered an area of 1 cm$^2$. To prepare the substrate for the backside imaging it was chemically thinned and polished to a thickness of 100 µm. The device contained standard circuitry used in commercial circuits and had a photosensitive electrostatic protection device at the input to an inverter chain with an area of around 150 µm$^2$. Eight n-doped silicon fingers bounded by atomically sharp metal were located in the active region (Fig. 2b). The fingers had widths of 4.5 µm and were separated by gaps of 500 nm. The tips of the $n$-doped structures contained a 3×3 matrix of tungsten vias, which were spaced at a pitch of 1.25 µm and had approximate diameters of 100 nm.

The laser-generated photocurrent was measured between ground and a pin connected to the active region [13]. The device remained unpowered at all times. The sample was mounted on a computer-controlled motorized 3-axis translation stage (ASI MS-2000), which had a (16½ × 23 × 9) cm travel range with a minimum physical step of 10 nm.

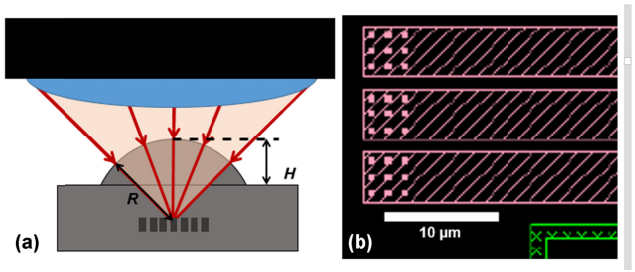


Fig. 2. a) Design of the SIL showing the definition of its height, $H$ and radius, $R$; b) design schematic showing the $n$-doped silicon finger structures in the photosensitive area of the IC.

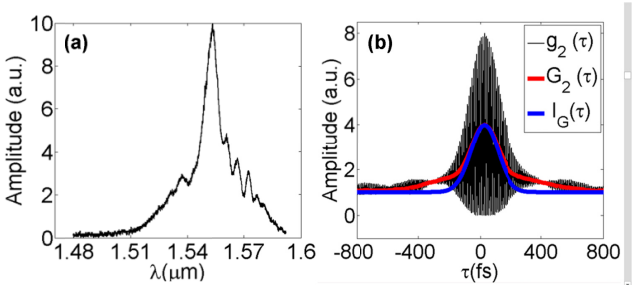


Fig. 3. Characterization of the Er:fiber laser showing (a) the optical spectrum and (b) the interferometric autocorrelation profile ($g_2(\tau)$, black) at the output. The FWHM pulse duration was 144 fs, inferred from a Gaussian envelope ($I_G(\tau)$, blue) fitted to the fringe-averaged autocorrelation ($G_2(\tau)$, red).

### B. Pulse Duration Measurements

Before conducting pulse duration measurements using the device itself, the laser operation was characterized by measuring its spectral distribution (Fig. 3a) and the autocorrelation at the laser output (Fig. 3b). The two-photon autocorrelation was recorded using a silicon photodiode and the spectrum was measured with a real-time laser spectrum analyzer. The autocorrelation shows moderate chirp because dispersion compensation in the fiber laser system was adjusted to minimize the pulse durations measured inside the IC rather than directly after the laser.

From the output of the Michelson interferometer the laser pulses were guided through the TOBIC microscope to the device layer of the IC, which acted as the nonlinear detector for the autocorrelation measurement. The two-photon photocurrent was detected and recorded using a digital oscilloscope in a way similar to that reported previously [17, 18]. Autocorrelations recorded in this way form the basis of the results in this paper and an example is shown in Section 3.

### C. Optical Resolution Measurements

An edge response at the silicon-metal transition of one of the finger structures shown in Fig. 2 was used to evaluate the lateral spatial resolution of the nonlinear imaging system. The TOBIC photocurrent falls from high to low when the laser focus moves from the semiconductor region and onto the metal region. This signal response is a combination of the point spread function (PSF) and the physical edge function. As the physical edge is a step function (the metal edge is atomically sharp), the intensity of the signal can be described as the integral of a Gaussian function [19]. The PSF full width at half maximum (FWHM) diameter was determined by using a least-squares minimization to fit a normalized Gaussian error function, erf($r$), to the data. The FWHM of the underlying Gaussian function gives the resolution limit of the system. Example data are shown in Fig. 4, indicating a resolution of 345 nm.

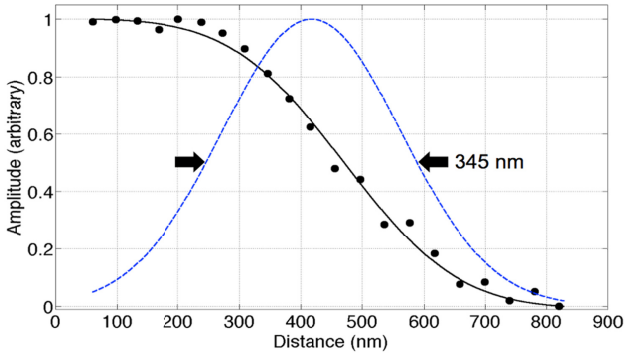


Fig. 4. Data showing a least-squares Gauss-error fit obtained from a line-cut of a TOBIC image of an $n$-doped silicon finger edge.

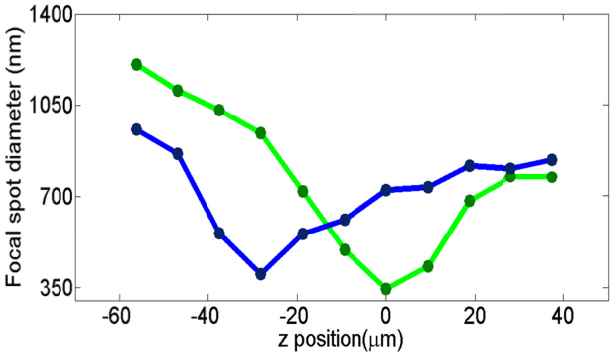


Fig. 5. Resolution values obtained while changing the laser beam focal position relative to the sample. Blue line: closed aperture results; green line: open aperture.

Resolution measurements were performed as the device was moved through the focal plane of the microscope. Two datasets were recorded, one with an unrestricted pupil (Fig. 5, open aperture) and a second with the aperture before the pupil reduced in diameter (Fig. 5, closed aperture). The zero position corresponds to where the PSF FWHM was smallest (a value of 345 nm), and values of $z > 0$ indicate moving the sample further from the objective lens. The presence of spherical aberration causes the focal position corresponding to the minimum PSF FWHM diameter to shift when the aperture is closed, and this is reflected in the data in Fig. 5. The data also show a small broadening of the PSF FWHM due to the decrease in NA when the aperture is closed. In the following section we proceed to correlate this spatial behavior with time-domain measurements based on two-photon autocorrelation.

## 3. RESULTS AND ANALYSIS

### A. Data Analysis Methodology

In a two-photon microscope the autocorrelation signal recorded by nonlinear gating within the sample itself provides two distinct pieces of information. As already introduced, the pulse duration estimated from the autocorrelation width delivers insights into the chromatic and spatial aberrations, but the autocorrelation intensity at zero delay is also correlated with the peak intensity at the focus, which is sensitive to both spatial and temporal distortions. Correspondingly, our analysis is based on two parameters: *1.* the pulse duration estimated from the two-photon absorption (TPA) fringe-averaged autocorrelation, $G_2(\tau) = \langle g_2(\tau) \rangle$; and *2.* the maximum amplitude of $G_2(\tau)$. The aim of the analysis is to understand how the minimum pulse duration and the maximum autocorrelation signal amplitude vary as a function of the defocusing. In order to estimate $G_2(\tau)$, from the fringe-resolved interferometric autocorrelation traces, $g_2(\tau)$, we Fourier-transformed $g_2(\tau)$ then applied a low-pass filter to extract the fringe-averaged function, $G_2(\tau)$. The resulting $G_2(\tau)$ profile (Fig. 6, red) was fitted with a Gaussian, $I_G(\tau)$ (Fig. 6, blue) to obtain estimates of the FWHM pulse durations, assuming Gaussian pulse intensity profiles and a deconvolution factor of $\sqrt{2}$. The absence of exact overlap between $G_2(\tau)$ and $I_G(\tau)$ simply reflects the fact that the pulse shape is not perfectly Gaussian.

The autocorrelation amplitude was defined as the peak value of $G_2(\tau)$ with respect to the base line (see Fig. 6.). The same filtering and fitting criteria were applied to measure the pulse duration and the autocorrelation amplitude as a function of focal position, generating corresponding datasets describing the variations of pulse duration and autocorrelation amplitude with defocus.

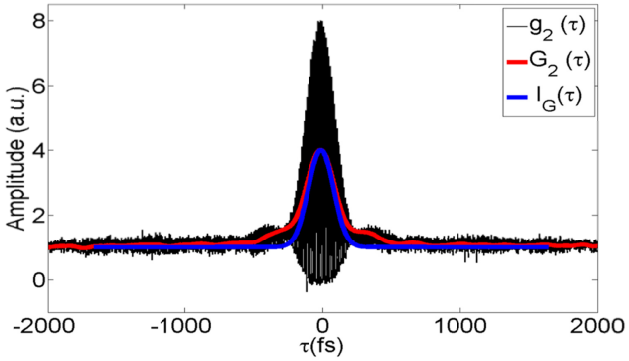


Fig. 6. Interferometric autocorrelation ($g_2(\tau)$, black) measured at the focus of the microscope, shown with the fringe-averaged autocorrelation ($G_2(\tau)$, red) and corresponding Gaussian fit ($I_G(\tau)$, blue).

### B. Experimental Results and Discussion

A near-infrared Plan APO Mitutoyo 20× long working distance microscope objective was used in all the experiments to focus the laser beam. This objective had a wavelength correction from the visible to near-infrared (1800 nm) and was corrected for an infinite conjugate, i.e. a plane wavefront incident on the objective.

We analyzed the behavior of two distinct optical systems as the device was scanned through the focal plane. The first system comprised the 20× microscope objective (MO) and the central SIL described in Section 2, and employed an adjustable aperture ("closed aperture") located in front of the objective lens, while the second system was identical but did not include an aperture. For comparison, an experiment with no SIL is presented in Section 3.

#### *1. Objective lens and SIL with a closed aperture*

The results are presented in Fig. 7. The relative focal position for $z$=0 was located at the maximum of the Gaussian fitting of the autocorrelation amplitude. Polynomial fitting, to the pulse durations shown in Fig. 7a, indicates that the minimum duration is located at $z$ = 90 μm. The solid black circles indicate our experimental data, obtained with the procedures described in Sections 2 and 3, and the black line is a second-order polynomial fit using a least squares fit. The blue dashed lines indicate the prediction bounds of the lower and upper values of the associated interval, defined by the uncertainty around the predicted fit. The level of certainty for our calculations is 90%. The data points outside the prediction bounds (red stars) were excluded from the fitting process, for instance the point at around $z$ = -90 μm in Fig. 7a.

In Fig. 7b, the experimentally measured autocorrelation amplitude is plotted as a function of defocus, together with a least-squares Gaussian fit to the data. It can be seen that the points fit well to the Gaussian, where the maximum amplitude is located at $z$ = 0 μm.

Defining the maximum autocorrelation signal amplitude to correspond to $z$ = 0 μm, we observed that the shortest pulse duration occurred at $z$ = 90 μm, a difference of 90 μm. This result indicates a problem with either spherical aberration or propagation time difference (PTD), or both [4], where PTD describes the temporal broadening of the pulse introduced by chromatic aberration.

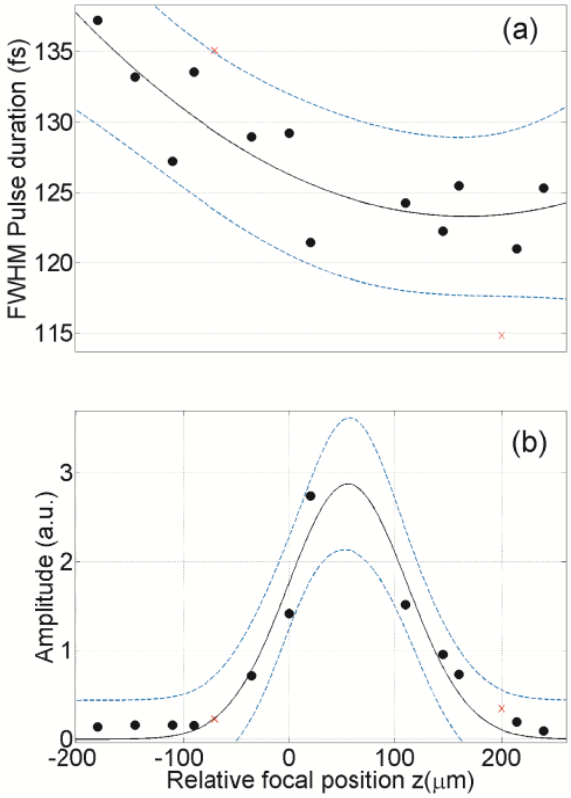


Fig. 7. Effects of defocusing for a system comprising an objective lens, SIL and a closed aperture. (a) Pulse-duration dependence on defocus, where the solid black circles are experimental data and the solid black line is a second-order polynomial fit. The interval delineated by the blue dashed lines indicates the prediction bounds with a level of certainty of 90%. (b) Autocorrelation amplitude dependence on defocus, where the solid black circles are experimental data and the black line is a Gaussian fit. The blue dashed lines indicate the 90% certainty bounds as in (a).

#### *2. Objective lens and SIL with no aperture*

Treating the data in the same way as described in Section 3.B.1, a second-order polynomial fit (Fig. 8a.) revealed that the position for the shortest pulse duration with the aperture removed was shifted to $z$ = 105 μm. As before, the relative focal position for $z$ = 0 was also defined at the maximum of the Gaussian fitting of the autocorrelation amplitude (Fig. 8b.). Again, this result indicates a problem with either spherical aberration or chromatic aberration, or both.

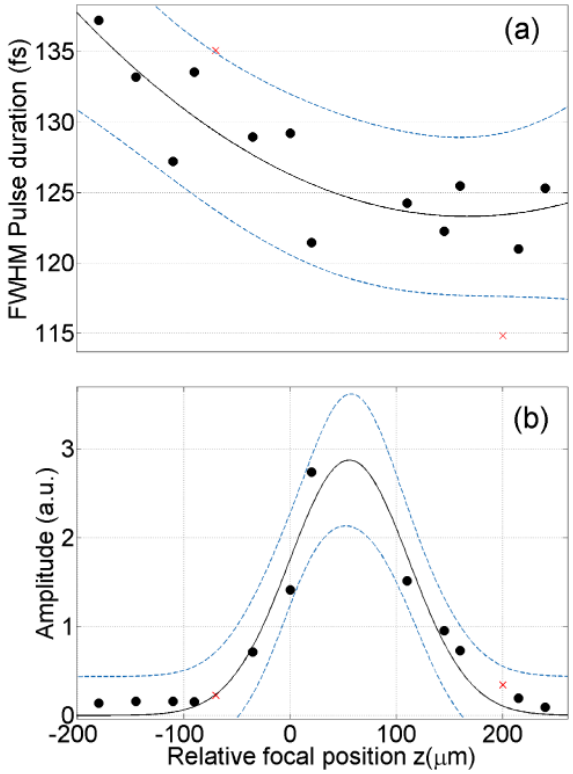


Fig. 8. Effects of defocusing for a system comprising an objective lens, SIL but no aperture. (a) Pulse-duration dependence on defocus, and (b) autocorrelation amplitude dependence on defocus. For definitions of symbols and lines see Fig. 7.

### *3. Objective lens with no SIL or aperture*

The analysis was repeated for a final time using data obtained with only the objective lens and with no SIL or aperture. In Fig. 9a, the pulse duration is plotted as a function of relative focal position *z*. In Fig. 9b the experimentally measured autocorrelation amplitude is plotted as a function of relative focal position *z*, together with a least-squares Gaussian fit to the data.

A second-order polynomial fit reveals that pulse duration changes very little with defocus which can be contrasted with the results using the SIL (Fig. 7 and Fig. 8) whereas the Gaussian fit to the autocorrelation amplitude shows the maximum amplitude located at z=0 μm.

### *4. Discussion*

Previously published modeling results from García-Martínez *et al.* [4] showed that the maximum autocorrelation signal amplitude is located at the position where spherical aberration is the smallest, which in turn gives the position for the best spatial resolution. In other words, by locating the maximum autocorrelation signal amplitude, the best spatial resolution position will be located. The same authors also showed that the positions corresponding to the minimum pulse duration and the maximum autocorrelation amplitude always coincide for an aberration-free lens, whereas a difference in positions indicates the presence of aberrations or group velocity dispersion, GVD. With these theoretical results in mind, the difference in the positions of minimum pulse duration and maximum autocorrelation signal amplitude with a closed aperture (Fig. 7.) and without an aperture (Fig. 8.) indicate that chromatic aberration, spherical aberration or GVD are present. Assuming that the objective lens is an optical system highly corrected for spherical aberration and chromatic aberration, the aberrations must therefore arise from either the SIL or from an aberrated incident wavefront on the objective lens or both.

The modeling in [4] uses two approximations: (1) scalar diffraction theory and, (2) the slowly-varying envelope approximation, which states that the bandwidth of the pulse, $\Delta\omega$, is smaller than the angular frequency of the carrier, $\omega_0$, i.e., $\Delta\omega/\omega_0 << 1$. The numerical apertures, NA, for the systems presented in Fig. 8 and Fig. 9 are 1.46 and 0.42 respectively. In Fig. 7 the NA is slightly smaller than the NA in Fig. 8. Only the system with the NA of 0.42 is well described by the scalar diffraction theory, whereas the other two systems with high numerical apertures are not. The second approximation is satisfied in all cases, since the ratio between the bandwidth and the angular frequency of the carrier of the pulses is $\Delta\omega/\omega_0 = 0.019$, assuming 120 fs @ 1.55 μm pulses modulated by a Gaussian envelope. The experimental results presented in Fig. 9a for the objective lens with no SIL show very little change of pulse duration with defocus, which can be contrasted with the results using the SIL (Fig. 7 and Fig. 8). Previous experiments reported in the literature [20,21], with lenses that satisfied both approximations, showed that large monochromatic aberrations and defocus do not change pulse duration, so the experimental results presented in Fig. 9a agree with previous experimental results. From these results we cannot conclude if the incident wavefront on the objective lens is well corrected or not. On the other hand, the other two experiments with the objective lens and SIL with a closed and open aperture show a change in pulse duration along *z*, so we can conclude that the SIL induces the change in pulse duration along *z*.

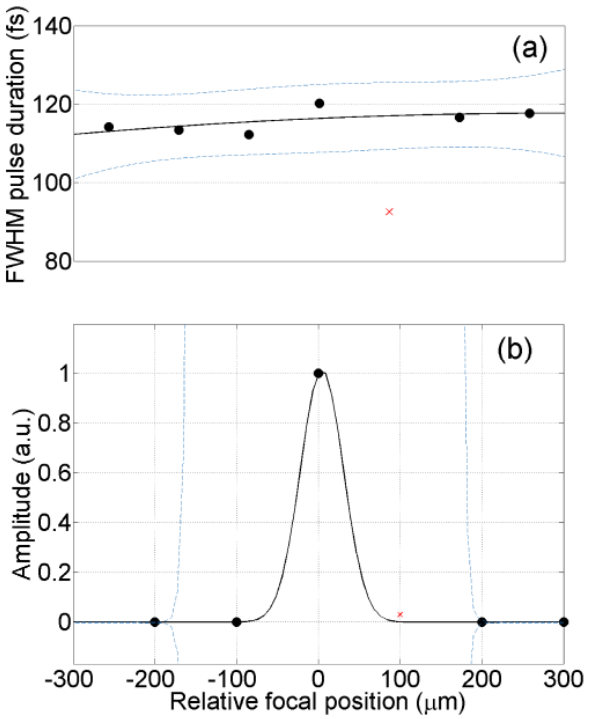


Fig 9. Effects of defocusing for a system comprising an objective lens with no SIL or aperture. (a) Pulse-duration dependence on defocus, and (b) autocorrelation amplitude dependence on defocus. For definitions of symbols and lines see Fig. 7.

The SIL is 2 mm in radius but only 1.73 mm in thickness (+0.1 mm of substrate) so it is not quite operating in the hemispherical condition (1.83 mm as opposed to 2 mm). A ray tracing simulation through an objective lens having NA=1.46 and a diameter of 8.4 mm (not

presented in this paper) showed that the transverse ray aberration at 1.55 μm introduced by the SIL is about one wavelength. This lens will also introduce some chromatic aberration and group velocity dispersion due to the deviation from the hemispherical condition. On the other hand, a poorly corrected incident wavefront on the objective lens will produce an aberrated wavefront incident on the SIL, which in turn will increase even more the aberration introduced by not exactly satisfying the hemispherical condition. In the experiment the GVD introduced by the thickness of the SIL material is compensated but a variation of GVD across the aperture may remain. On the other hand, since the SIL increases the numerical aperture of the system up to 1.46, scalar diffraction theory is not perfectly satisfied anymore, and we cannot expect the peak of the autocorrelation amplitude to be coincident with the position for minimum spherical aberration unless this aberration is well corrected. Further work to extend the modeling to high numerical apertures is being carried out.

Finally, although the SIL introduces spherical and chromatic aberrations and a variation of GVD, we cannot exclude the presence of large aberrations in the incident wavefront on the objective lens potentially introduced in the system by the use of singlet lenses in a beam expanding telescope prior to the objective lens.

## 4. CONCLUSIONS

Our results are the first example of applying the theoretical insight from [4] in a nonlinear microscope. The approach offers a potentially simple means of minimizing whole-system aberrations by iteratively optimizing the objective lens position and the illumination wavefront until the minimum difference has been found between the positions of minimum pulse duration and maximum autocorrelation signal. The inclusion of a motorized stage to actuate the objective position, together with a liquid-crystal spatial light modulator (SLM) to control the wavefront before the objective lens would form the basis for this approach. Autocorrelation data recorded in only a few seconds would be sufficient to construct amplitude and pulse duration scans similar to those in Fig. 8. The difference in the positions of minimum duration and maximum intensity would provide a metric on which an optimization strategy could be based. A simple hill-climbing approach in which the SLM was used to apply defocus or another low-order aberration could be investigated. Stochastic optimization methods such as simulated annealing or genetic algorithms would offer a more general solution [22], in which the SLM would be used to randomly perturb the wavefront and gradually drive the error towards smaller values. In this way the optical system before the microscope could be adjusted to minimize its contribution to the aberrations of the whole system, leaving only the intrinsic aberrations of the sample and objective-SIL lens combination.

**Funding.** Dirección General de Asuntos del Personal Académico, Universidad Nacional Autónoma de México (DGAPA, UNAM) (PAPIIT-IG100615). The Intelligence Advanced Research Projects Activity (IARPA) via Air Force Research Laboratory (AFRL) (FA8650-11-C-7104).

## References

1. Rodrigo Aviles-Espinosa, Jordi Andilla, Rafael Porcar-Guezenec, Omar E. Olarte, Marta Nieto, Xavier Levecq, David Artigas, and Pablo Loza-Alvarez, "Measurement and correction of in vivo sample aberrations employing a nonlinear guide-star in two-photon excited fluorescence microscopy," Biomed. Opt. Express **2**, 3135-3149 (2011).
2. Delphine Débarre, Martin J. Booth, and Tony Wilson, "Image based adaptive optics through optimisation of low spatial frequencies," Opt. Express **15**, 8176-8190 (2007).
3. H. Song, R. Fraanje, G. Schitter, H. Kroese, G. Vdovin, and M. Verhaegen, "Model-based aberration correction in a closed-loop wavefront-sensor-less adaptive optics system," Opt. Express **18**, 24070-24084 (2010).
4. L. García-Martínez, M. Rosete-Aguilar, and J. Garduño-Mejía, "Gauss-Legendre quadrature method used to evaluate the spatio-temporal intensity of ultrashort pulses in the focal region of lenses," Appl. Opt. **51**, 306–315 (2012).
5. M. Born and E. Wolf, Principles of Optics, 7th ed. (Cambridge University Press, 2005).
6. C. Xu and W. Denk, "Two-photon optical beam induced current imaging through the backside of integrated circuits," Appl. Phys. Lett. **71**, 2578–2580 (1997).
7. C. Xu and W. Denk, "Two-photon optical beam induced current imaging through the backside of integrated circuits," J. Appl. Phys. **86**, 2226–2231 (1999).
8. C. Xu, L. M. F. Chirovsky, W. S. Hobson, J. Lopata, W. H. Knox, J. E. Cunningham, W. Y. Jan and L. A. D'Asaro, "Two-photon photocurrent imaging of vertical cavity surface emitting lasers," Appl. Phys. Lett. **76**, 1510–1512 (2000).
9. K. A. Serrels, C. Farrell, T. R. Lundquist, D. T. Reid, and P. Vedagarbha, "Solid-immersion-lens-enhanced nonlinear frequency-variation mapping of a silicon integrated-circuit," Appl. Phys. Lett. **99**, 193103 (2011).
10. K. A. Serrels, K. Erington, D. Bodoh, C. Farrell, N. Leslie, T. R. Lundquist, P. Vedagarbha, and D. T. Reid, "Two-photon laser-assisted device alteration in silicon integrated-circuits," Opt. Express **21**, 29083 (2013).
11. M. Rutkauskas, C. Farrell, C. Dorrer, K. L. Marshall, T. Crawford, T. R. Lundquist, P. Vedagarbha, K. Erington, D. Bodoh, and D. T. Reid, "Two-photon laser-assisted device alteration in CMOS integrated circuits using linearly, circularly and radially polarized light," Microelectronics Reliability **60**, 62–66 (2016).
12. K. A. Serrels, E. Ramsay, P. A. Dalgarno, B. D. Gerardot, J. A. O'Connor, R. H. Hadfield, R. J. Warburton and D. T. Reid, "Solid immersion lens applications for nanophotonic devices," J. Nanophotonics **2**, 021854 (2008).
13. E. Ramsay, N. Pleynet, D. Xiao, R. J. Warburton and D. T. Reid, "Two-photon optical-beam-induced current solid-immersion imaging of a silicon flip chip with a resolution of 325 nm," Opt. Lett. **30**, 26–28 (2005).
14. M. Baba, T. Sasaki, M. Yoshita, H. Akiyama, "Aberrations and allowances for errors in a hemisphere solid immersion lens for submicron-resolution photoluminescence microscopy," J, Appl. Phys. **85**, 6923 (1999).
15. Y. Lu, T. Bifano, S. Ünlü, B. Goldberg, "Aberration compensation in aplanatic solid immersion lens microscopy," Opt. Express. 21, 28189-97 (2013).
16. J. C. M. Diels, J. J. Fontaine, I. C. McMichael, and F. Simoni, "Control and measurement of ultrafast pulse shapes (in amplitude and phase) with femtosecond accuracy," Appl. Opt. **24**, 1270-1282 (1985).
17. D. T. Reid, W. Sibbett, J. M. Dudley, L. P. Barry, B. Thomsen, and J. D. Harvey, "Commercial semiconductor devices for two photon absorption autocorrelation of ultrashort pulses," Appl. Opt. **37**, 8142-8144 (1998).
18. E. Ramsay, D.T. Reid, "Investigation of the two-photon optical beam induced current effect in silicon integrated circuits," Optics Communications **221**, 427–433 (2003).
19. S. P. Ippolito, B. B. Goldberg, and M. S. Ünlü, "High spatial resolution subsurface microscopy," Appl. Phys. Lett. **78**, 4071-4073 (2001).
20. M. González-Galicia, J. Garduño-Mejía, M. Rosete-Aguilar, N.C. Bruce and R. Ortega-Martínez, "Effects of primary spherical aberration, coma, astigmatism, and field curvature on the focusing of ultrashort pulses: Gaussian illumination and experiment," J. Opt. Soc. Am. A 28 (10), 1990-1994, (2011).
21. M.Rosete-Aguilar, J. Garduño-Mejía, and Neil. C. Bruce, "Focusing ultrashort laser pulses with achromatic doublets," SPIE Newsroom 10.1117/2.1201504.005926 (2015).
22. O. Katz, E. Small, Y. Bromberg and Y. Silberberg, "Focusing and compression of ultrashort pulses through scattering media," Nature Photon. **5**, 372-377 (2011).